Applications of Nuclear Quadrupole Resonance Spectrometry to Analytical Chemistry

Harry D. Schultz

Morgantown Energy Research Center, Bureau of Mines, U. S. Department of the Interior, Morgantown, West Virginia 26505

(Received 25 November 1970; revision received 9 February 1971)

Since Dehmelt [H. Dehmelt and H. Krüger, Naturwiss. **37**, 11 (1950)] observed the first pure quadrupole resonance signal in 1949, this technique has been developed to a high degree of sophistication for the investigation of bonding and structural features in compounds. Most of the early data were obtained on organic halides. More recently, NQR has been used to research inorganic bonding characteristics such as π and σ bonding in nitrogen compounds and transition metal complexes. The technique has also been extensively developed for mineralogical research, including recent applications for quantitative analysis of specific minerals in natural ore deposits. The major developments in instrumentation which were made in an effort to solve these problems are discussed.

INDEX HEADINGS: Nuclear quadrupole resonance spectroscopy; Analytical applications; Instrumentation.

INTRODUCTION

Nuclear quadrupole resonance (NQR) is used to investigate the character of chemical bonds in solids, including the influence of impurities, defects, etc. The occurrence of quadrupole energy levels in crystals is caused by the interaction between nonspherical nuclei and the nonuniform electric field of the lattice or molecule. The quadrupole resonance frequency depends on the type of resonating quadrupolar nucleus and the electric field gradient of the crystal or molecule. Since the absorption frequency for various isotopes is different, and since the specific frequency depends on the type of bonding, this method can be used for qualitative chemical analysis (Figs. 1 and 2). Peak height or peak area measurements can be related to quantitative analysis. The multiplicity of the spectrum may provide data for drawing conclusions concerning the crystal structure and bonding of molecules.

Nuclear quadrupole resonance signals can be observed only in crystalline solids; however, liquids can be frozen and studied at low temperatures. If the crystal lattice is disturbed (paramagnetic centers, impurities, irradiation, disordered), the width of NQR lines increases. (The influence of paramagnetic centers is complex. Paramagnetic centers can reduce the spin–spin relaxation time, T_2, causing a decrease in saturation. Consequently, the signal intensity can increase as the line width decreases.) Consequently, the NQR method can be used for inspecting the quality of the crystal system. This is especially valuable in synthesizing new chemical compounds, where the occurrence of NQR signals indicates that the product obtained is of high crystal lattice purity.

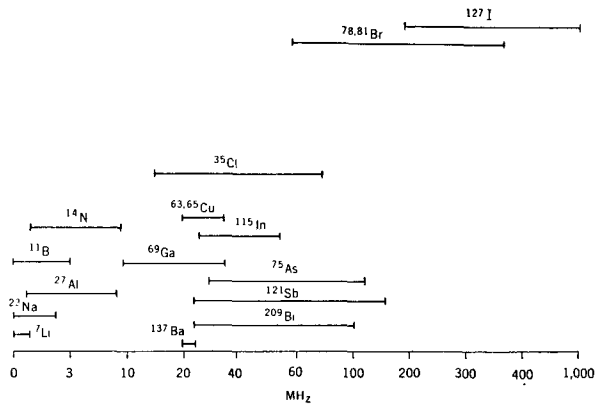

FIG. 1. NQR frequencies for various isotopes.

I. THEORY

An external radio frequency field precisely corresponding to the energy difference of nuclear states will

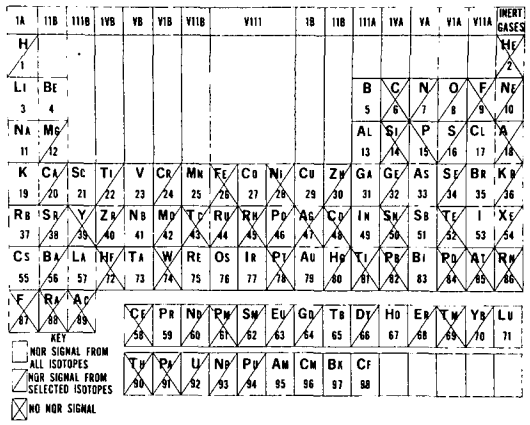

FIG. 2. NQR periodic table (taken from Wilks Scientific Corp. resume of the NQR-1A nuclear quadrupole resonance spectrometer).

Table I. Quadrupole resonance frequencies.

I	Secular energy equation	$\nu(\eta=0)$	$\nu(\eta\neq0)$
1	···	$3eQq_{zz}/4$	$3eQ(q_{zz})/4\cdot(1\pm\eta/3)$
$\frac{3}{2}$	$E^2-3\eta^2-9=0$	$eQq_{zz}/4I(2I-1)$	$eQ(q_{zz})/2\cdot(1+\eta^2/3)^{\frac{1}{2}}$
$\frac{5}{2}$	$E^3-7(3+\eta^2)E^2$ $-2O(1-\eta^2)=0$	$eQq_{zz}/2I(2I-1)$	$\nu_1=3eQq_{zz}/20\cdot(1+1.09259\eta^2-0.63403\eta^4)$ $_2=3eQ(q_{zz})/10\cdot(1-0.20370\eta^2+0.16215\eta^4)$
$\frac{7}{2}$	$E^4-42(1+\eta^3/3)E^2$ $-64(1-\eta^2)E$ $+105(1+\eta^2/3)^2=0$	$3eQq_{zz}/4I(2I-1)$	$\nu_1=eQ(q_{zz})/14\cdot(1+3.63333\eta^2-7.26070\eta^4)$ $_2=2eQ(q_{zz})/14\cdot(1-0.56667\eta^2+1.85952\eta^4)$ $_3=3eQ(q_{zz})/14\cdot(1-0.1000\eta^2-0.01804\eta^4)$
$\frac{9}{2}$	$E^5-11(3+\eta^2)E^3$ $-44(1-\eta^2)E^2$ $+44/3(3+\eta^2)^2E$ $+48(3+\eta^3)(1-\eta^2)=0$	$3eQq_{zz}/2I(2I-1)$	$\eta_1=eQ(q_{zz})/24\cdot(1+9.03333\eta^2-45.69070\eta^4)$ $_2=2eQ(q_{zz})/24\cdot(1-1.338095\eta^2+11.72240\eta^4)$ $_3=3eQ(q_{zz})/24\cdot(1-0.1857\eta^2-0.12329\eta^4)$ $_4=4eQ(q_{zz})/24\cdot(1-0.08095\eta^2-0.004258\eta^4)$

cause forced transitions between these states. The transitions are accompanied by absorption of energy from the radio frequency field. The frequency absorbed in NQR is proportional to the quadrupole moment (Q) of the nucleus, to the nuclear spin (I), and to the field gradient (q) of the molecule or crystal.

The electric quadrupole moment measures the deviation from spherical symmetry of a nucleus. Only nuclei with nuclear spins greater than one-half have electric quadrupole moments.

The electric field gradient (q) is the negative second derivative of the electrostatic potential, v, at the nucleus produced by nearby charges. The tensor components along the X, Y, and Z axes are q_{xx}, q_{yy}, and q_{zz}. If q is axially symmetric with $Z(\partial^2v/\partial X^2=\partial^2v/\partial Y^2)$ and since $q_{xx}+q_{yy}+q_{zz}=0$, only two quantities (q_{zz} and η) are needed to define the field gradient tensor, where the asymmetry parameter

$$\eta=(q_{xx}-q_{yy})/q_{zz}. \tag{1}$$

A nucleus with a quadrupole moment situated in an inhomogeneous electric field possesses a potential energy which depends upon the orientation of the quadrupole moment with respect to the electric field. The quadrupole coupling between different energy states is directly proportional to the nuclear quadrupole coupling constant (eQq). Although the energy states are electrical in origin, the transitions are caused by the interaction between the magnetic component of the rf field and the magnetic moment of the nucleus.

In an axially symmetric field ($\eta=0$), the energy arising from a nucleus of moment Q in the field of gradient q is defined by

$$E_m=\frac{eqQ[3m^2-I(I+1)]}{4I(2I-1)}, \tag{2}$$

where m is the magnetic quantum number, which takes $2I+1$ values between I and $-I$. The quadrupole resonance frequency is given by

$$\nu_r=\frac{3eQq}{4hI(2I-1)}[2(m_I)-1]. \tag{3}$$

Consequently, $\nu_r=3eQq/4h$ for $I=1$, $eQq/2h$ for $I=\frac{3}{2}$, etc.

In a nonsymmetric environment ($\eta\neq0$) the energies of the different quadrupole states are not defined by Eq. (2). Table I lists the resonance frequency equations for various nuclear spin systems when $\eta\neq0$. The quadruple coupling constant (eQq) can be used to estimate the ionic character and hybridization of covalent bonds. The electric field gradient (q_{zz}) is sensitive to the structure of the electron shells. The asymmetry parameter (η) can be used to estimate the π-electron concentration near the atom in certain instances.

A. Intensity of NQR Signals

The intensity of NQR signals depends upon (a) the angle between the axis of the electric gradient and the applied rf field, (b) the population excess in the lower state of the transition, (c) the spin–lattice relaxation time T_1, and (d) the transition probability, $(H_1\mu/I)^2$. Energy absorption is via coupling of the magnetic dipole μ of the nucleus to the magnetic vector H_1 of the rf field. Population excess (very small in absolute terms) is proportional to $h\nu/kt$; and thus strong signals occur when the quadrupole coupling constant is large, the absolute temperature is low, and T_1 is short.

A transition will not be observed if the line width is too great. Factors affecting line width are (a) internal molecular motion, (b) lattice vibrations, (c) saturation of the transition, (d) magnetic coupling to other nuclei, and (e) defects or strains in the crystal structure. The most important factor is the last since it can result in line broadening to such an extent that the signal is completely lost in the oscillator noise.

II. INSTRUMENTATION

Most nuclear quadrupole resonance spectrometers are based on either a regenerative (continuous wave) or super-regenerative (quenched) oscillator–detector.

A. Super-Regenerative

A coil and variable air condenser in parallel make up the tank circuit of an rf oscillator–detector. The spectrum is scanned by rotating the condenser. In a

super-regenerative oscillator,[1,2] the driving force is periodically cut off, and reactivated when the oscillations have almost died away. This is the quenching cycle. An absorbing sample (placed in a vial inside the coil) affects the rate of decay of oscillations and hence the exact level remaining at the moment of buildup. Good spectrometer gain stability can be achieved by maintaining a constant ratio of coherent oscillations to residual noise at the moment of buildup. Too much coherence leads to poor sensitivity, while too little results in a very noisy signal. Peterson and Bridenbaugh,[3] at Bell Laboratories, were the first to build an NQR spectrometer in which the noise from the oscillator was continuously monitored and used to control the length of time the oscillator was inactive. If an NQR spectrometer is to scan a wide frequency range while maintaining a constant noise level, this type of automatic control is essential.

The spectrum produced by a super-regenerative oscillator contains the principal frequency (center peak) and side bands because of the mixing of the principal frequency with the quench frequency. If the frequency is modulated and phase-sensitive detection is used, then the side band responses are suppressed.[4,5]

B. Regenerative

In a regenerative oscillator,[6–8] the sample is inserted into the oscillator coil and becomes an element of the resonant circuit. When the frequency of the oscillations in the circuit corresponds to the frequency between the quadrupole energy levels, the sample absorbs energy from the circuit. The sensitivity of regenerative oscillators over a wide frequency range is often poor compared to that of the super-regenerative spectrometers. However, a regenerative system is better for line shape, multiple structure, and relaxation time studies.

C. Spin–Echo

A third type of NQR instrumentation is that of the quadrupole spin–echo technique.[9–11] If the sample is subjected to two rf pulses separated by time τ, then 2τ sec after the first pulse an echo signal is produced which is the result of the interaction of the damping signals of nuclear induction. The spin–echo method combined with double resonance techniques permits NQR studies at low frequencies because the double resonance does not require a Boltzmann population difference for the second spin system.

Oscillator circuits employing field effect transistors (FET's)[12] are gradually replacing circuits using vacuum tubes. The noise figure (0.5 dB) of field effect transistors is a factor of 4 better than vacuum tubes. Use of these devices in the oscillator circuit, audio amplifier, and filter circuits yields better signal-to-noise ratios. Also, these circuits operating at low voltage avoid the problems of hum and pickup associated with high voltages. A disadvantage of using FET's is the requirement of a large sample.

During 1967, Wilks Scientific Corporation sold the first commercial NQR instrument, based on the design of Peterson.[3] Decca Radar Limited of England has entered the market with a design following that of Smith,[5] and Varian offers information on NQR experiments performed on their wide-line nuclear magnetic resonance spectrometers.

III. CHEMICAL APPLICATIONS

A great deal of NQR data has been interpreted to provide a critical test for field gradients as calculated from molecular orbital theory, and for point charge calculations for ionic lattices. However, NQR is a useful technique for a variety of studies of solid-state chemistry such as the character of the chemical bond, the number of physical and chemical nonequivalent atom positions in the crystalline structure, the detection of phase transitions, the determination of purity of a material, and the application to qualitative and quantitative analysis. Chemical nonequivalence is typified by a greater frequency shift than physical nonequivalence. As will be seen from the discussions on chemical bonding, the influence of pi and sigma bonds on absorption frequencies is significant.

The first attempt to correlate electronic structure with nuclear quadrupole coupling constants was made by Townes and Dailey[13] on a series of dihalides. From these studies they formulated the following equations

$$eQq_{(\mathrm{mol})} = (1-s+d)(1-i)eQq_{(\mathrm{at})}, \quad (4)$$

$$eQq_{(\mathrm{mol})} = (1-s+d)(1-i)+2(1+c)eQq_{(\mathrm{at})}, \quad (5)$$

where i is the ionic character, s and d are the amount of s and d hybridization in the halide bond, c is a constant (approximately 0.25 to account for positive ionization), and $eQq_{(\mathrm{at})}$ is the coupling constant of an isolated atom. Equation (4) is specific for correlating eQq values for chlorine compounds and Eq. (5) is for other halogens. Townes and Dailey concluded that the major contribution to the electric field gradient comes from p electrons in the valence shell because p orbitals have spherical symmetry.

A plot of ionicity, $1-P_q$, vs electronegativity difference, X_h-X_m, on a series of diatomic halides shows that for electronegativity differences greater than two, bonding is essentially 100% ionic in support of the Townes and Dailey result.[14] In this instance ionicity is defined by

$$P_q = eQq_{(\mathrm{mol})}/eQq_{(\mathrm{at})}, \quad (6)$$

$$1-P_q = \tfrac{1}{2}(X_h-H_m) \quad \text{for } X_h-X_m<2. \quad (7)$$

The halogen bond character of 24 alkyl halides has been calculated using a modified form of the Townes–Dailey equation

$$eQq_{(\mathrm{mol})}/eQq_{(\mathrm{at})} = \mathrm{I}-s+d-i-\mathrm{II}, \quad (8)$$

where I is the single bond character and II is the double bond character. Calculating the sum total of s and d hybridization, it is found that the average values

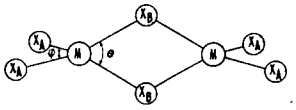

FIG. 3. Structure of group III halide molecules.

are 13.6% for C–Cl bonds, 8.6% for C–Br bonds, and 1.9% for C–I bonds in agreement with the Townes–Dailey hybridization rules.[15]

When correlating molecular structures of a given family of compounds, it is convenient to define a quantity

$$Up = eQq_{(\mathrm{mol})}/eQq_{(\mathrm{at})}, \tag{9}$$

called the "number of unbalanced p electrons." Considerable insight can be gained from studying families of compounds by utilizing the above equations where some of the parameters remain constant or are zero.

A. Halogens

More NQR data have been collected on chlorine compounds than all others combined (Figs. 1 and 2) because standard radio frequency oscillators have maximum sensitivity in the range of 10–70 MHz (most ^{35}Cl frequencies are between 20–50 MHz), and chlorine resonances are not usually saturated by high rf power. Since the initial studies on dihalides by Townes and Dailey, a vast amount of NQR data has been collected on halogen compounds. Only a few examples will be offered here to familiarize the reader with the type of results which can be deduced from NQR spectral data.

1. Group III Halides

The halogen spectrum of group III trihalides[16–18] on $AlBr_3$, $GaCl_3$, InI_3, etc., consists of three resonances, two being closely spaced at approximately 20 MHz and lying well above the third at approximately 15 MHz. The difference in the high field frequencies establishes a physical crystalline inequivalence around a set of chemically identical atoms. Bond angles calculated from the asymmetry parameter by

$$\eta_M = 3\cos\theta \tag{10}$$

indicates a dimerized molecule containing two halogen bridge bonds (Fig. 3). Calculated Up values demonstrate the halogen bridge bonds are weaker (longer) than the others in agreement with x-ray results.

2. Group IV Halides

The percent ionic character and percent single bond and double bond character of the group IV halides have been extensively investigated by the NQR method.[19–22] The double bond character is greatest for Si halides, showing that the greater π character in Si compounds shortens the Si–X internuclear distance and hence decreases the dipole moment. Another indication of greater π character of the Si–X bonds is demonstrated by the fact that Up is less for the Si halides than for any of the other M halides. Also, a plot of eQq vs electronegativity difference of the central metal atom and the halide atom gives a linear relationship. Since Si–X compounds show the smallest eQq values, the Si atom should be the most electropositive of the group IV atoms. Thus the following electronegativity order is postulated as accounting for the linear relationship between eQq and $(X_x - X_m)$: C > Ge > Sn > Si.

3. Transition Metal Halides

Covalency calculated from the contributions of the antibonding state to the p charge density [magnetic transferred hyperfine interaction (THFI)], and from quadrupole coupling in transition metal halides[23] is compared. Assuming that contributions from p electrons to the quadrupole interaction dominate, then

$$f_Q = (eQq)_{\mathrm{crystal}}/\mathrm{n_h}(eQq)_{\mathrm{atom}}, \tag{11}$$

Table II. Covalency determined by THFI and NQR in transition metal halides.

Compound	A_s(10^{-4} cm^{-1})	f_s(%)	$A_\sigma - A_\pi$(10^{-4} cm^{-1})	$f_\sigma - f_\pi$(%)	$\nu Q = (eqQ/2h) \times (1+1/3n^2)^{\frac{1}{2}}$ (Mc/sec)	fQ(%)
$CuCl \cdot 2H_2O$	7.8	0.50	5.0	9.8	9.0	15.8
$CdCl_2$:Cu^{++}	9.5	0.61	4.5	8.8		
$CuF_2 \cdot 2H_2O$	86	0.55	24	5.5		
$CoCl_2$					2.56	4.7
$CoCl_2 \cdot 2H_2O$	5.6	1.08	0.8	4.7	5.2	9.4
$CoCl_2 \cdot 6H_2O$					5.5	10.0
$KCoF_3$	26		8			
$KMgF_3$:Co^{2+}	23	0.48	6	2.9		
$FeCl_3$					2.37	4.3
AgCl:Fe^{3+}	2.8	0.90	0.5	4.9		
$FeCl_3$					10.12	18.2
$KMgF_3$:Fe^{3+}	24.0	0.76	2.9	3.3		
$CrCl_2$					8.52	15.5
$CrCl_3$					12.92	23.4
K_2NaCrF_6	−1.1	−0.02	−7.2	−4.9		
VCl_3					9.40	17.0
$TiCl_2$					4.17	
$TiCl_3$					7.39	13.4
$(NH_4)_2PtCl_6$:Ir^{4+}			8.8	−4.3		
K_2PtCl_6					26.02	47.0

where f_Q is the excess hole density of the ligand and p orbital, $n_h = 1, 2, \cdots$ is the number of holes in the molecular orbital before bonding.

Similarly, the fractional amount of spin density in the chlorine $3p$ orbital is

$$f_\sigma - f_\pi = 2S(A_\sigma - A_\pi/A_{3p}), \qquad (12)$$

where $A_\sigma - A_\pi$ is the antisotropic THFI. The isotropic THFI, A_s, is calculated by a Hamiltonian $A_s I \cdot S + (A_\sigma - A_\pi)(\frac{3}{2}I_z S_z - \frac{1}{2}I \cdot S)$. When symmetry does not permit spin density to be transferred to the π orbitals (octahedral d^8 or d^9 configuration), then $f_\sigma - f_\pi$ reduces to f_σ. When σ spin–transfer does not occur (d^1, d^2, or d^3), $A_\sigma - A_\pi$ determines f_π. Once f_σ or f_π is determined then the coefficients of the ICAO–MO theory can be calculated and f_Q related to the antibonding wave function. Table II summarizes the eQq and THFI data obtained on transition metal halides. Several conclusions can be drawn from these data.

(a) f_Q measures the holes in both spin paired and unpaired orbitals, whereas $f_\sigma - f_\pi$ measures only the holes associated with the unpaired orbitals. However, both f_Q and $f_\sigma - f_\pi$ measure the excess p holes in the bond direction and roughly increase and decrease simultaneously as a measure of covalency.

(b) The fluoride f_s values demonstrate that a small amount of hyperfine interaction of the metal atom $3d$ orbitals to the fluorine $2s$ function exist. The f_s values for chlorine and fluorine are small, indicating that the halogen atom bonding functions are not appreciably hybridized with s functions.

(c) The f_σ values are larger for Cl than for F, demonstrating that fluorides are more ionic than chlorides.

(d) A comparison of eQq values for $CrCl_2$, $CrCl_3$; $FeCl_2$, $FeCl_3$; and $TiCl_2$, $TiCl_3$ shows that the higher halides are more covalent than the lower ones.

(e) The eQq values decrease in the series $CrCl_3$, $FeCl_3$, $TiCl_3$ because the t_{2g} metal orbitals empty and π delocalization becomes more prevalent as the number of π electrons decrease.

4. Hexahalides of Heavy Atoms

The NQR spectra of a series of hexahalides of complex ionic compounds of the general formula R_2MX_6 have been interpreted in terms of the covalency of the metal–ligand bonds.[24] The ionic character of these compounds was obtained by use of the Townes–Dailey equations with the exception that the halogen bonding orbitals were assumed to have 15% s character. In cases where only outer d orbitals are present (Se, Te, Sn, and Pb compounds) the ionic nature is very high, consistent with bond formulation involving only valence s and p orbitals. The higher quadrupole frequencies of Se/Te compounds compared to Sn/Pb compounds are a result of two extra electrons in the group IV series (Table III).

When the d orbitals are partially occupied and form part of the valency shell (transition metal complexes), then the metal–halogen bonds are much more covalent (higher resonance frequencies). However, dative bonding by the lone pair electrons of the halogen atoms can lead to a reduction in coupling constant and an increase in the ionic character of the metal–halogen bond.

Assuming that the number of electrons migrating from the halogen ion to the central metal ion is proportional to the number of electronic vacancies in the t_{2g} orbitals, Nakamura has extended the Townes–Dailey method to include π bonding. Pi is proportional

Table III. NQR data on hexahalides. M is an average of K^+, Cs^+, NH_4^+, and $N(CH_3)_4^+$.

Hexahalide	$X = {}^{35}Cl$ ν	eQq/Mcs	$1-i$	ρ	$X = {}^{79}Br$ ν	eQq/Mcs	$1-i$	ρ	$X = {}^{127}I$ ν	eQq/Mcs	$1-i$	ρ
K_2PtX_6	26.021	52	56	0.64	202	406	62	0.28	407	1360	70	−0.20
K_2PdX_6	26.75	53.2	57	0.58	205.34	411	63	0.22	···	···	···	···
K_2SeX_6	20.58	41.2	44	1.36	173	346.2	53	0.82	···	···	···	···
NH_4SeX_6	20.877	41.8	45	1.30	172.623	345.2	53	0.82	···	···	···	···
Cs_2SeBr_6	···	···	···	···	177.44	354	54	0.76	···	···	···	···
K_2TeX_6	···	···	···	···	135.670	271	42	···	154 302	1022 1011	52	···
NH_4TeCl_6	15.137	30.3	32	2.08	···	···	···	···	···	···	···	···
M_2TeX_6	···	···	···	···	129.946 134.258	273.5 266.18	42	1.48	154	···	52	0.88
Cs_2TeBr_6	···	···	···	···	135.962	271.92	···	···	···	···	···	···
$N(Me)_4TeBr_6$	···	···	···	···	142.58	285.16	···	···	···	···	···	···
K_2SnX_6	···	31.5	34	···	130.5	261	40	1.60	···	884	45	···
$(NH_4)_2SnBr_6$	···	···	···	···	1269 at −72°C	253	39	1.66	···	···	···	···
K_2WX_6	10.22 at 22.5°C	20.4	0.22 (0.57)	0.58	···	···	···	···	···	···	···	···
K_2ReX_6	13.9	27.9	0.28 (0.55)	0.70	115	231.34	34 (61)	0.34	123 246	822.21	57 (68)	0.08
K_2OsX_6	16.897	33.8	0.38 (0.53)	0.80	···	···	···	···	···	···	···	···
K_2IrX_6	20.841	41.7	0.45 (0.53)	0.80	···	···	···	···	···	···	···	···
$(NH_4)_2PbX_6$	···	34.5	0.37	···	···	···	···	···	···	···	···	···

Table IV. ^{14}N quadrupole resonance.

Compound	eQq	η(%)
N_2	4.65	0
N_2 in quinone clathrate	4.6	
HCN	4.0183	0.85
ClCN	3.219	0.0157
BrCN	3.27	0.006
ICN	3.40	0
NH_3	3.5705	0
ND_3	3.2308	0
$CO(NH_2)_2$	3.507	32.3
$C_3N_3Cl_3$	4.083	1.7
CCl_3CN	4.0521	0.53
$K_2Zn(CN)_4$	4.139	0.00
$K_2Cd(CN)_4$	4.1988	0.00
$K_2Hg(CN)_4$	4.0475	0.00
$K_3Cu(CN)_4$	3.9639	2.94
$K_2Pt(CN)_4 \cdot 3H_2O$	3.467	3.2 (av)
$K_3CO(CN)_6$	3.684	3.0 (av)
$Hg(CN)_2$	3.9513	
$NaNO_2$	5.792	40.5 (av)

to $6-n$, where n is the number of electrons in the antibonding t_{2g} orbital. Since $n=2$, 3, 4, and 5 in W^{4+}, Re^{4+}, Os^{4+}, and Ir^{4+} complexes, $\pi=0.22$, 0.16, 0.11, and 0.05, respectively. If these π values are included to calculate covalency, then numbers are obtained which are appreciably higher than the values calculated when only pure σ bonding is considered.

For K_2PtCl_6 the π orbital is completely filled and no π delocalization of the halogen lone pair electrons occurs. However, for K_2IrCl_6, π delocalization becomes apparent and increases from osmium to tungsten as the number of electrons in the antibonding π orbital decreases by one as the series is descended.

Support for the π bonding hypothesis comes from a consideration of the temperature coefficient of the quadrupole coupling constant. The temperature coefficient

$$\frac{\partial \nu}{\partial T}=\left(\frac{\partial \nu}{\partial T}\right)_V+\left(\frac{\partial \nu}{\partial v}\right)_T\left(\frac{\partial v}{\partial T}\right)_P \qquad (13)$$

is usually negative. However, positive temperature coefficients were obtained for K_2ReCl_6 ($d\nu/dT$, kc/deg $=0.13$), K_2WCl_6 (0.44), and K_2ReBr_6 (2.8). Since the temperature coefficient is normally negative, the major term $(\partial\nu/aT)_V$ is negative. Theoretically this term is based on thermal vibration of anions, but does not take into account the thermal expansion of the lattice. As the thermal vibration of the complex ion increases, the overlap of the σ orbital of the central metal ion with the P_z orbital of the halogen decreases, leading to decreased covalent character of the metal–ligand bond; consequently, the field gradient q and the quadrupole frequency decrease with increasing temperature. A positive temperature coefficient results when this effect predominates over the usually negative temperature coefficient as is the case with K_2ReCl_6, K_2WCl_6, and K_2ReBr_6 where the metal–ligand bonds involve high π bond character. Because of the cylindrical symmetry of p orbitals, the t_{iu} π bonding is only slightly affected by bonding vibrations and is neglected in the above analysis.

Brown *et al.*[25] take exception to the assumption that the extent of π bonding is a function of the varancies in the metal d_π orbitals. Arguing that the number of electrons transferred per d_π vacancy is inversely proportional to the difference in optical electronegativity, then the number of electrons transferred per d_π vacancy should decrease in the series $Pt<Ir<Os<Re<W$. Force constants for the metal IV series as calculated from Raman and ir spectra actually increase and can be correlated with an increase in covalency of the metal–chlorine bond, giving support to the observed NQR data.

The hexahalides offer an example where the maximum chemical information may be obtained from quadrupole resonance frequencies. Unfortunately, few such examples exist in the NQR literature.

B. Nitrogen Quadropole Resonance

The quadrupole coupling constants of the ^{14}N nucleus are small, seldom being more than 6 MHz, and the intensities of the pure quadrupole resonance lines are weak. Consequently, an extremely sensitive spectrometer is required to obtain good results. The long relaxation time T_1, frequently encountered with ^{14}N resonance leads to difficulty in detecting a resonance. For example, the ν_1 line for urea has a T_1 of 40 sec and the ν_2 line has a T_1 of 78 sec at 77 K. These long relaxation times make for easy saturation of the lines. In addition, most ^{14}N measurements have been made using magnetic field modulation, which becomes ineffective for polycrystalline samples if the asymmetry parameter is large. However, by using frequency modulation, asymmetry up to 40.5% has been reported. Further improvement in the circuitry for ^{14}N studies is very desirable. These are the reasons that data on this nucleus have been obtained so slowly. The difficulty of studying these low frequencies is offset by the large variety of different bonding structures present in compounds of the ^{14}N isotope.

Also, for a nucleus with a spin $I=1$, both η and eQq can be obtained from the resonance frequencies on polycrystalline powder. The pure quadrupole resonance frequencies are given by

$$\nu_0=\tfrac{1}{2}h\eta\cdot eQq, \qquad (14)$$

$$\nu_\pm=\tfrac{3}{4}h\eta eQq(1\pm\eta/3). \qquad (15)$$

The frequency ν_0 is small and rarely observed, but can be useful in pairing the $\nu_\pm$ frequencies when multiplet spectra are observed. Nitrogen is found in a variety of bonding types: three single bonds; one single, one double; triple bond (cyanide); isocyanide; conjugated heterocyclic rings. Since each type has characteristically different frequencies (Table IV) the NQR spectrum qualitatively determines the chemical nature

and location of a nitrogen atom, its physical crystalline structure, and provides an excellent test for the wave functions used in theoretical calculations of bond character.

The quadrupole coupling constant decreases as π bonding increases in metal–cyano complexes[26] because of the migration of electrons of the central metal atom into the vacant antibonding π molecular orbitals of the cyano group. For example, metal–ligand bonds in the platinum and cobalt complexes ($eQq = 3.5$–3.7) have a greater extent of d_π–p_π bond character than in the zinc, cadmium, mercury, and copper complexes ($eQq = 4.0$–4.7).

In the simple cyanides, a quadrupole coupling constant of 3.8–4.0 MHz is obtained for ^{14}N in hydrogen cyanide[27] and alkyl cyanides where a CN group is bonded to the rest of the molecule by a σ bond. By contrast, a halogen $X{-}C{\equiv}N$, or sulfur $R{-}S{-}C{\equiv}N$ atom bonded to the carbon atom of the cyano group yields a quadrupole coupling constant in a range from 3.2 to 3.6 MHz, corresponding to the contribution from resonance structures $X^+{=}C{=}N^-$ and $R{-}S^+{=}C{=}N^-$.

C. Minerals

Nuclear quadropole resonance spectra can be used to analyze the chemical and crystal structure of minerals such as the pyramidal coordination complexes, RX_3, where R is As, Sb, Bi, and X is S or O. Qualitative correlation of the coupling constant to the electron state of the atom R can be related to the geometry of these complexes. Quadrupole shifts are due to the changes in the effective charge of the atoms R and X. Donor–acceptor bonds, induction, and steric effects are the causes of changes in the effective charge of atoms in R_2X_3 type minerals. If atom R is carrying a positive charge, polarity of the principal bonds decreases resulting in a reduction of the field gradient at the nucleus R. The coupling constant is sensitive to small gradient changes resulting from weak bonds of the donor–acceptor type. In realgar (As_4S_4) the values of eQq (178.44, 182.10, 184.10, and 185.92 MHz) for the four nonequivalent positions of As atoms are due to a slight difference in their field of force because of the effect of donor–acceptor bonds.[28] In orpiment, As_2S_3, (the product of realgar alteration) weak homo-atomic bonds, As–As, are identifiable by means of pulsed NQR echo signals[29] and are assigned to dative bonding between As atoms of two adjacent chains.

Coordination polymer compounds are other examples of the effect of donor–acceptor bonds. For example, antimonite contains $(Sb_4S_6)_n$ macromolecules regarded as dimers of Sb_2S_3 linked by a pair of equidistant bridge bonds. Because of the redistribution of electron densities, two of the four SbS_3 polyhedrons in the polymer are strongly distorted ($\eta = 38.10\%$) and the coordination polyhedron becomes a semi-octahedron.[30] In realgar, another example of a coordination polymer, the lowest of the four eQq values (178.44 MHz) is greater than the highest value for orpiment (143.88 MHz). This is caused by the fact that the S–As–S–As chains in orpiment (regarded as condensates of realgar half-molecules As_2S_2) have S as the bridging atom, as compared to metallic Sb in antimonite. With such a structure the number of bonds in each atom remains unchanged; however, the number of sulfur atoms in the polymer increases from two to three, with AsS_3 polyhedrons being formed.

The induction effect (polarization) is realized in compounds with two or more electropositive atoms. For example, in the series antimonite (Sb_2S_3), pyrargyrite (Ag_3SbS_3), and bourmonite ($CuPbSbS_3$), the eQq values for ^{121}Sb increase from 318.0 to 332.3 to 376.2 MHz, respectively.[31] This is explained by the growing number of electropositive sites which influence the field gradient of the atom R, thus changing the quadrupole coupling constant. Another example of the induction effect is that of monoclinic bismuth oxide, $\alpha \cdot Bi_2O_3$. When boron atoms (B_2O_3) are emplaced into the monoclinic lattice of $\alpha \cdot Bi_2O_3$, a small frequency shift results for the ^{209}Bi nuclei.[32] A growth of the asymmetry parameter indicates a distortion of the Bi_2O_3 lattice. Also, the boron atoms lower the ionic nature of the BiO bonds. These factors are responsible for the resonance shift to lower frequencies.

The steric effect is much like polarization. For example, the crystal lattice of natural pyrargyrite (Ag_3SbS_3) includes some As atoms in the form of proustite (Ag_3AsS_3). The shift to lower resonance for the additive AsS bonds in pyrargyrite reveals more ionic character than for that in pure proustite (Ag_3AsS_3).[33]

The high sensitivity of NQR shifts from different crystal structures makes it ideal to study mineralogical order–disorder phenomena.[34] This is difficult by other spectroscopic techniques because the data are an average for both standard and distorted unit cells. For example, x-ray diffraction indicates that all polyhedrons in bourmonite are distorted to the same extent as implied by the interatomic distances. Nuclear quadropole resonance data reveal that one polyhedron is almost symmetrical ($\eta < 0.2\%$), while

Table V. ^{35}Cl NQR of $CHCl_3$ and CCl_4 complexes.

Compound	ν(MHz at 77 K)	Compound	ν(MHz at 77)
$CHCl_3$	38.253	CCl_4	40.465–40.817 (15 lines)
	38.308	$CCl_4 \cdot (C_2H_5)_2O$	40.132
$CHCl_3 \cdot (C_2H_5)_2O$	37.627		40.181
	37.896		40.495
$CHCl_3 \cdot 2(C_2H_5)_2O$	37.272		40.907
	37.608		41.097
	37.874	$CCl_4 \cdot 2(C_2H_5)_2O$	40.494
	38.160		40.738
$CHCl_3 \cdot 3(C_2H_5)_2O$	37.274	$CCl_4 \cdot (CH_3)_2CO$	40.280
	37.946		40.380
	38.169		40.696
$ChCl_3 \cdot (CH_3)_2CO$	37.310		40.970
	37.752	$CCl_4 \cdot pCH_4(CH_3)_2$	40.472
	37.650		40.689
$CHCl_3 \cdot C_6H_4(CH_3)_2$	37.814		
	37.842		

Table VI. NQR of miscellaneous complexes.

Compound	ν_x (MHz at 77 K)	ν_{Sb}	Compound	ν_x (MHz at 77 K)	
CBr_4	265.45		$SnCl_4$	24.294	
	266.06			24.226	
	266.4–267.06			24.140	
	267.97			23.719	
	268.30		$SnCl_4 \cdot 2(C_2H_5)_2O$	19.473	
	269.25			19.435	
$CBr_4 \cdot p$-xylene	264.95		$SnCl_4 \cdot C_6H_5NO_2$	23.08 (av of six lines)	
	269.18		$POCl_3$	28.9835	
	319.46			28.9378	
	321.83		$SnCl_4 \cdot POCl_3$	30.213	
$AsCl_3 \cdot POCl_3$	29.208			30.117	
	29.168			21.146	
	29.154			19.807	
	25.481			19.035	
	25.125		$AsCl_3$	25.406	
	24.799			25.058	
$HgCl_2$	22.873			24.968	
	22.521		$SbCl_5 \cdot CH_3CN$	24.99	32.47, 64.87 (^{121}Sb)
$HgCl_2 \cdot C_4H_8O_2$	21.196			26.37	19.70, 39.43, 59.06 (^{123}Sb)
$SbCl_5$	18.76–30.50 (eight lines)	27.93–54.22 (seven lines)			
$SbCl_5 \cdot POCl_3$	24.44–30.64 (six lines)	34.05, 58.37 (^{121}Sb)			
		25.30, 34.48, 53.76 (^{123}Sb)	C_6F_5Cl	39.410	
			$C_6F_5Cl \cdot C_6H_6$	38.717	
			$C_6F_5Cl \cdot$ Mesitylene	38.684	
			$C_6F_5Cl \cdot$ Anilene	38.640	
			$C_6F_5Cl \cdot$ Triethylene	39.284	
			$C_6F_5Cl \cdot$ Toluene	39.158	
				39.312	

the other is highly distorted ($\eta = 22.8\%$). A widening of the quadrupole resonance signal is a result of disordered minerals, dislocations being the most effective. In low symmetry crystals, dislocation is confined chiefly to the vicinity of nuclei with the higher value of the asymmetry parameter. The detection of nonstructural impurities in the parent matrices depends on their concentration, as the NQR spectrum would be identical with that of a standard specimen of the compound. The observation of structural impurities is more complicated as these distort the matrix system, and often both the host and emplacement compounds undergo spectral changes, including resonance broadening.

Proustite (Ag_3AsS_3) and pyrargyrite ($AgSbS_3$) exhibit restricted isomorphism. For instance, natural pyrargyrite containing 2% As gave a ^{75}As signal at 67.580 MHz compared with a 67.311-MHz signal for pure proustite. Also, the width of the resonance line of additive proustite is approximately 300 KHz compared to a width of 24 KHz for a standard specimen of proustite.

$\alpha \cdot Bi_2O_3$ alloyed with B_2O_3 shows the effect of emplacement on the width of resonance lines. Boron atoms bring about a marked widening of the ^{209}Bi resonance line, mostly for a single position of the Bi atoms, corresponding to the highest value of the asymmetry parameter ($\eta = 38\%$). Because dislocations interact with impurities and create concentration clouds, a definite correlation exists between the asymmetry parameter and the distribution of the impurity.

Temperature relationships between the spin–lattice relaxation (T_1) and the resonance frequencies correlate for individual functional groups. In antimonite, one of the R–X bonds in SbS_5 ($\eta = 38.1\%$) is 2.49 Å, appreciably shorter than the other bonds. The value

Table VII. X(^{35}Cl, ^{81}Br), ^{121}Sb, ^{123}Sb NQR complexes of SbX with organic compounds.

Compound	ν_x	$\nu_{^{123}Sb}$	$\nu_{^{121}Sb}$	Compound	ν_x	$\nu_{^{123}Sb}$	$\nu_{^{121}Sb}$
$SbCl_3$	20.9077	59.728	39.108	$SbBr_3$	137.429 (α)	···	
	19.3047				144.488		
$2SbCl_3 \cdot C_6H_6$	20.509	59.774	38.566		136.885 (β)		
	20.459	59.602	37.117		137.621		
	20.349			$2SbBr_3 \cdot C_6H_5$	141.899	33.568	50.717
	20.068				142.614		
	18.749			$SbBr_3 \cdot C_6H_5 \cdot CH_3$	···	···	49.500
	18.655			$SbBr_3 \cdot C_6H_5 \cdot C_2H_5$	135.880	31.817	48.992
$SbCl_3 \cdot C_6H_5CH_3$		57.312	36.860		138.842		
$SbCl_3 \cdot C_6H_5C_2H_5$	20.076	58.689	37.988		140.330		
$SbCl_3 \cdot o$-$C_6H_5CH_3$		57.074		$SbBr_3 \cdot o$-$C_6H_4(CH_3)_2$		28.627	46.323
$SbCl_3 \cdot m$-$C_6H_5CH_3$		58.495		$SbBr_3 \cdot m$-$C_6H_4(CH_3)_2$		···	46.574
$SbCl_3 \cdot p$-$C_6H_5CH_3$		58.257		$SbBr_3 \cdot C_6H_5 \cdot OCH_3$		31.342	50.194
$SbCl_3 \cdot C_6H_5OCH_3$		58.457	36.426	$SbBr_3 \cdot C_6H_5OC_2H_5$		30.189	49.610
$SbCl_3 \cdot C_6H_5OC_2H_5$		56.063	35.167				

Table VIII. NQR data of complexes between iodides and sulfur.

Compound	ν_M	ν_{I_1}	ν_{I_2}	eQq	η
AsI_3	29.338	207.023	395.979	1330.23	0.1891
$AsI_3 \cdot 3S_8$	49.501	227.543	455.059	1516.86	0.007
SbI_3	25.406	174.356	254.637	895.83	0.565
$SbI_3 \cdot 3S_8$	37.461	184.151	367.023	1226.25	0.03
SnI_4	···	203.470	406.902	1363.28	0.000
		204.490	408.988	1360.04	0.002
$SnI_4 \cdot 2S_8$	···	204.019	408.008	1360.04	0.002
		206.784	413.153	1377.40	0.028
$SnI_4 \cdot 4S_8$	···	201.961	403.897	1346.3	0.00
		202.036	404.081	1346.9	0.00
		206.853	413.238	1377.7	0.30
		213.148	···	···	···

of T_1 for this type of complex is approximately three times that for the symmetrical complexes where $\eta = 0.8\%$

D. Charge–Transfer Complexes

Research on charge–transfer complexes[35–39] is of value to catalysis, semiconductors, and pharmacological studies. For example, chloroform and carbon tetrachloride form molecular complexes (Table V) which are strong narcotics. As hydrogen atoms are replaced with chlorine atoms in methane, the strength of narcotic action increases. The NQR spectrum of pure chloroform was obtained at 38.253 and 38.308 MHz. When $CHCl_3$ complexes are formed, the multiplicity of the NQR spectrum increases and the resonance frequencies decrease. The frequency shift in chloroform complexes is greater than in carbon tetrachloride complexes, establishing the fact that $CHCl_3$ is a stronger acceptor than CCl_4, in agreement with calculations by the MO–LCAO method for bonding orbitals.

Also, chlorpromazine, an electron donor, is successful in treating schizophrenia. Many believe that narcosis is caused by charge–transfer complex formation resulting in the disturbance of metabolism in the protoplasm.

Tables V–VIII summarize some pure quadrupole resonance studies on molecular complexes.

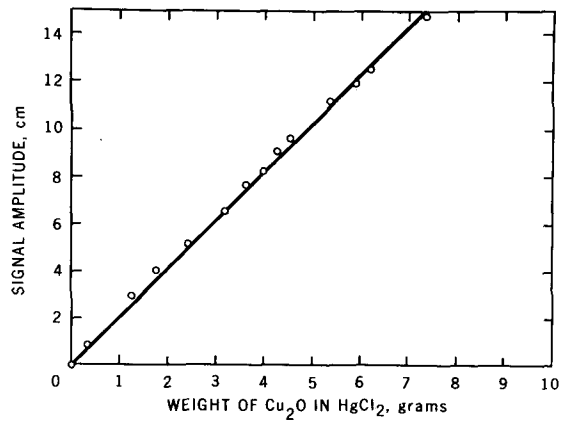

FIG. 4. Calibration curve for 65 Cu (24.6 MHz) in Cu_2O.

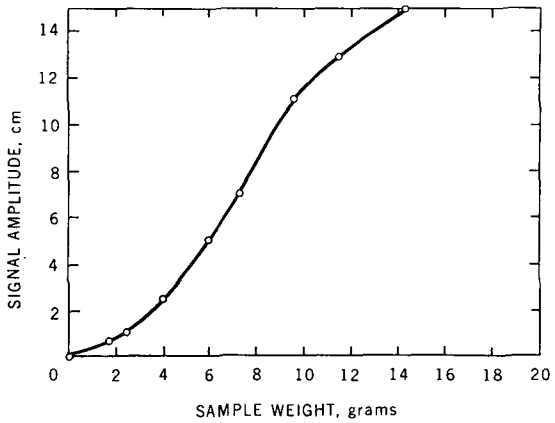

FIG. 5. Effect of quantity of sample in rf coil.

The advantage of NQR for the study of charge–transfer complexes is that the direction and extent of electron transfer can be determined. One cannot only establish the strength of donors and acceptors, but also the composition of the complex. In some cases, complete transfer of one electron takes place; in other cases varying amounts of charge–transfer takes place from the π electron of one molecule to the vacant π orbital of another.

E. Quantitative Analysis

Correlation charts for correlating NQR frequencies to molecular and crystalline structures are becoming rather common.[40] Qualitative identification of unknown compounds can be determined from their frequency position as discussed in the previous sections.

In contrast to the qualitative features of a spectrum, quantitative analysis applications of NQR are only recently being made. The quantitative data as discussed in this section were taken using a super-regenerative oscillator.

The intensity of the NQR signal is a linear function of concentration (Fig. 4).[41,42] However, only the region corresponding to the volume of the oscillator coil gives a linear response although a weak nonlinear signal is obtained along the axis immediately outside the coil area (Fig. 5). For a given quantitive analysis, both standard and unknown samples must occupy a fixed volume within the same portion of the oscillator coil.

The signal-to-noise power ratio, P_s/P_η, is related to the voltage ratio, V_s/P_η, and thus to the weight, ω, of the sample by the following equation

$$(P_s/P_\eta)^{1/2} = V_s/V_\eta = Kz = K'\omega, \qquad (16)$$

where K, K' are dimensional constants, and z is the filling factor for the circuit (approximately equal to the coil volume covered by the sample).

The magnetic energy density is not uniform throughout the coil volume, being the least uniform near the ends of the coil solenoid. Consequently, a nonlinear relationship exists between signal-to-nosie voltage ratio and z at the ends of the rf coil. This is

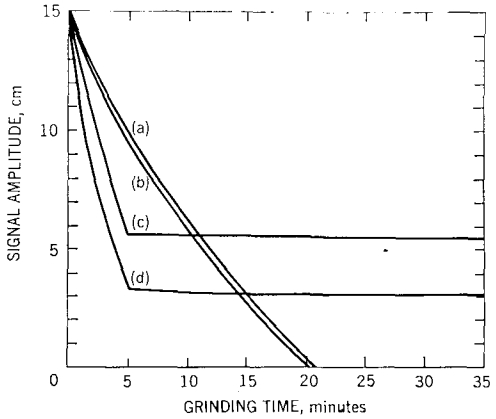

FIG. 6. Effect of tungsten carbide grinding on NQR signal; (a) cuprite ^{63}Cu at 26.5 MHz, (b) Cu_2O ^{63}Cu at 26.5 MHz, (c) $HgCl_2$ ^{35}Cl at 22.5 MHz, (d) $HgCl_2$ ^{35}Cl at 22.4 MHz.

borne out by the fall-off of signal peak amplitude at the end of the rf coil as demonstrated in Fig. 5 (end of coil).

The signal-peak amplitude is taken as the height of the center line. Area measurements obtained by perimeter tracings on the NQR signal give calibration lines of slightly less reproducibility and linearity than peak height measurements. The amplitude, A, of the resonance signal corresponds to the weight of the compound under investigation in the sample as follows

$$A = Kz = k\omega, \qquad (17)$$

where k is a constant equal to the slope of the calibration line.

When grinding is to be part of the analytical procedure, then the effect of the method of grinding on the signal amplitude of the specific compound under investigation should be determined before quantitative analysis is attempted. The ^{63}Cu signal at 26.5 MHz for both cuprite ore and synthetic Cu_2O is completely destroyed after 20 min of grinding in a tungsten carbide vial (Fig. 6). However, if hand grinding with a mortar and pestle or if agate vial grinding is employed, no reduction in signal intensity is observed. The restriction against vigorous grinding presents few analytical problems because an average value can be determined from several different selections of ore, or a mild grinding method can be employed. This is demonstrated in Table IX for five different selections of high purity cuprite ore. All samplings consistently gave values close to 100% Cu_2O.

Another, unique, quantitative application is based on the sensitivity of the NQR peak height to low levels of impurity (5–500 ppm) dissolved in solid solution in a sample. The amount of signal decrease depends on the number of nuclei thrown off resonance by the impurity center; this relationship is linear for low-impurity concentration. For example, the amount of p dibromobenzene (in the 0.1%–1% range) is a linear function of the integrated NQR signal.[43]

The electronic inductive effect characterized by values of Hammett's σ parameter have been quantitatively correlated with quadrupole resonance fre-

Table IX. Quantitative analysis of minerals by NQR.

Sample	Source	Weight of sample (g)	Weight of Cu_2O in cuprite, g (from 26.5 MHz)	Wt% Cu_2O in cuprite 26.5 MHz	Wt% Cu_2O in cuprite 24.6 MHz	Weight of As_2O_3 in arsenolite (from 116 MHz)	Wt% As_2O_3 in arsenolite (from 116 MHz)
Cuprite	Butte, Montana, No. 1	5.01	1.00	20.0			
Cuprite	Butte, Montana, No. 1	4.58	1.15	25.1	29.5		
Cuprite	Butte, Montana, No. 2	3.07	1.00	32.6	33.9		
Cuprite	Butte, Montana, No. 2	4.57	1.70	37.1			
Cuprite	Bisbee, Arizona, No. 1	4.03	0.90	20.9	21.2		
Cuprite	Bisbee, Arizona, No. 1	4.53	0.65	14.2			
Cuprite	Bisbee, Arizona, No. 2	6.52	6.50	99.7	99.5		
Cuprite	Bisbee, Arizona, No. 2	6.38	6.40	100.3			
Cuprite	Ajo, Arizona	6.89	7.00	101.6	99.1		
Cuprite	Ajo, Arizona	6.89	7.05	102.3			
Cuprite	Ajo, Arizona	6.79	6.95	102.4			
Cuprite	Ajo, Arizona	6.79	7.05	103.8			
Cuprite	Ajo, Arizona	5.70	5.60	98.2	99.4		
Cuprite	Burra, Australia	5.63	1.45	25.6			
Cuprite	Burra, Australia	6.21	1.50	24.2	24.8		
Arsenolite	Nevada, No. 1	4.43				1.011	22.8
Arsenolite	Nevada, No. 1	5.17				1.20	23.2
Arsenolite	Nevada, No. 2	5.25				2.804	53.4
Arsenolite	Nevada, No. 2	6.28				3.28	52.2
Arsenolite	Nevada, No. 3	4.57				1.109	21.9
Arsenolite	Nevada, No. 3	5.62				1.26	22.5

quencies of *chloro*-substituted benzene compounds.[44] Similar correlations have been made with Taft's polar subsituent parameter σ^* on *chloro*-benzene derivatives,[45] RCH_2Cl compounds and group IV halides.[22]

1. J. R. Whitehead, *Super-regenerative Receivers* (Cambridge U. P., New York, 1950).
2. J. D. Graybeal and C. D. Cornwell, J. Phys. Chem. **62**, 483 (1958).
3. G. E. Peterson and P. M. Bridenbaugh, Rev. Sci. Instrum. **35**, 698 (1964); A. C. Gilby, in *Spectrometry of Fuels*, edited by R. A. Friedel (Plenum, New York, 1970).
4. C. Dean and M. Pollak, Rev. Sci. Instrum. **29**, 630 (1958).
5. J. A. S. Smith and D. A. Tong, J. Sci. Instrum. **1**, 8 (1968).
6. N. Hopkins, Rev. Sci. Instrum. **20**, 401 (1949).
7. R. V. Pound and W. Knight, Rev. Sci. Instrum. **21**, 219 (1950).
8. T. C. Wong, Phys. Rev. **99**, 566 (1955).
9. J. Buchta, Rev. Sci. Instrum. **29**, 55 (1958).
10. T. P. Das and E. L. Hahn, *Nuclear Quadrupole Resonance Spectroscopy* (Academic, New York, 1958).
11. G. W. Smith, Phys. Rev. **149**, 346 (1966).
12. T. L. Viswanathan, T. R. Viswanathan, and K. V. Sanc, Rev. Sci. Instrum. **39**, 472 (1968).
13. C. H. Townes and B. P. Dailey, J. Chem. Phys. **17**, 782 (1949).
14. W. Gordy, Disc. Faraday Soc. **19**, 14 (1955).
15. B. P. Dailey, J. Chem. Phys. **33**, 1641 (1960).
16. R. G. Barnes and S. L. Segel, Phys. Rev. Lett. **3**, 462 (1959).
17. G. E. Peterson and P. M. Bridenbaugh, J. Chem. Phys. **51**, 233 (1969).
18. P. A. Casabella and P. J. Bray, J. Chem. Phys. **30**, 1393 (1959).
19. A. L. Allred and E. G. Rochow, J. Inorg. Nucl. Chem. **5**, 262 (1958).
20. J. M. Mays and B. P. Dailey, J. Chem. Phys. **20**, 1695 (1952).
21. A. L. Schawlow, J. Chem. Phys. **22**, 1211 (1954).
22. I. P. Biryukov and M. G. Voronkov, Teor. Eksperim. Khim. Akad. Nauk Ukr. SSR **1**, 373 (1965).
23. T. Fuke, J. Phys. Soc. Japan **18**, 1154 (1963).
24. M. Kubo and D. Nakamura, in *Advances in Inorganic and Radiochemistry*, edited by H. J. Emeleus and A. G. Sharpe (Academic, New York, 1966), Vol. 8, pp. 257–280.
25. T. L. Brown, W. G. McDugle, Jr., and L. G. Kent, JACS **92**, 3645 (1970).
26. R. Ikeda, D. Nakamura, and M. Kubo, J. Phys. Chem. **72**, 2982 (1968).
27. H. Negita, P. A. Casabella, and P. J. Bray, J. Chem. Phys. **31**, 730 (1959).
28. I. N. Pen'kov and I. A. Safin, Dokl. Akad. Nauk SSR **153**, 692 (1963).
29. I. N. Pen'kov and I. A. Safin, Proc. Acad. Sci. SSR **156**, 459 (1964).
30. I. A. Safin and I. N. Pen'kov, Proc. Acad. Sci. SSR, Phys. **147**, 815 (1962).
31. R. R. Sharma and T. P. Das, J. Chem. Phys. **41**, 3581 (1964).
32. I. N. Pen'kov and I. A. Safin, Fiz. Tverd. Tela **7**, 190 (1965).
33. I. N. Pen'kov and I. A. Safin, Soviet Phys. Solid State **6**, 1957 (1965).
34. I. N. Pen'kov and I. A. Safin, Dokl. Akad. Nauk SSR **161**, 1404 (1965).
35. O. Hassel and C. Romming, Quart. Rev. (London) **16**, 1 (1962).
36. V. Grechishkin and I. A. Kyunstel, Zh. Struckt. Khim. **5**, 53 (1964).
37. G. K. Semin, V. D. Shteingartz, and G. G. Yakobson, Zh. Struckt. Khim. **6**, 143 (1965).
38. Y. K. Maksyumin, E. N. Gur'yanova, and G. K. Semin, Zh. Struckt. Khim. **9**, 701 (1968).
39. Y. K. Maksyustin, T. A. Babushkina, E. N. Gur'yanove, and G. K. Semin, Theoret. Chim. Acta **14**, 48 (1969).
40. E. G. Brame, Anal. Chem. **39**, 918 (1967).
41. H. D. Schultz and C. Karr, Jr., Anal. Chem. **41**, 661 (1969).
42. S. Hacbobian, Aust. J. Chem. **15**, 21 (1962).
43. T. C. Wong, Phys. Rev. **99**, 566 (1955).
44. P. Biryokov and M. G. Voronkov, Coll. Czech. Chem. Commun. **32**, 830 (1967).
45. D. Beidenkapp and A. Weiss, J. Chem. Phys. **49**, 3933 (1968).

Future Articles

25th Anniversary

Commentaries by Evans, Strock, Von Hippel, Duffield, and Koch. Congratulatory letters by Brode and Cleveland.

Feature Articles

Recording Raman Spectra of Polymers—M. J. Gall, P. J. Hendra, D. S. Watson, and C. J. Peacock.

The Technique of Raman Spectroscopy: A State-of-the-Art Comparison to Infrared—H. J. Sloane.

Submitted Articles

Safety Interlock for Raman Spectrometer Laser Beam—A. M. Bartz, C. B. Pratt, and R. O. Kagel.

A Study of Solid State Anion Exchange between Some *p*-Aminophenol Hydrohalides and Twelve Alkali Halides by ir Spectroscopy—D. M. Drew and J. T. van Gemert.

Infrared Band Contours and PR Separations of Fluorinated Aromatics: 1,4-Difluorobenzene—H. D. Bist, M. M. Rai, and D. P. Khandelwal.

Vibrational Spectroscopic Study of 0,0-Dimethyl 0-(2,4,5-Trichlorophenyl) Phosphorothioate—R. Nyquist and W. Muelder.

Solution Luminescence of Anthraquinone, Naphthoquinone, and Some Derivatives at Room Temperature—B. S. Yamanshi and D. M. Hercules.

$\Delta Ms = \pm 2$ Transitions of Benzophenone and Derivatives in the Phosphorescent Triplet State Via Fast-Scan Flash-Synchronized ESR—B. S. Yamanashi, C. Mazza, and K. W. Bowers.

continued on p. 304

FEATURE AUTHOR

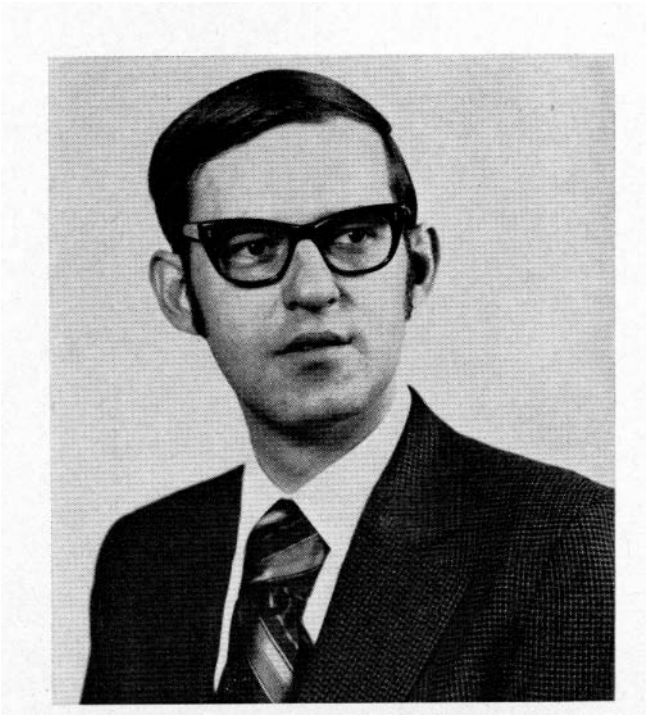

H. D. Schultz received a B.Sc. in Chemistry from West Virginia University, Morgantown, West Virginia, in 1964 under Professor George L. Humphrey. He has received graduate level training at both WVU and Carnegie–Mellon University, Pittsburgh, Pennsylvania. From 1964 to 1966 he engaged in the research of coal tar chemicals, plastics, and dyes by means of high resolution proton nuclear magnetic resonance and infrared spectroscopy while employed with the Koppers Research Center, Monroeville, Pennsylvania. With the United States Bureau of Mines at Morgantown, West Virginia, since 1966, Shultz has been active in the research of sulfur compounds and minerals identification in coal, as contributors to pollution and environmental health problems, using the techniques of pulsed nuclear magnetic resonance, pure quadrupole resonance, and electron spectroscopy for chemical analyses.

He is a member of the American Chemical Society, the Society of American Spectroscopists, and the Pittsburgh Spectroscopy Society.

ERRATUM

The Editors of Applied Spectroscopy and the Publications Division of AIP apologize for the inadvertent transposition of the photographs of Neil T. McDevitt and Freeman F. Bentley on page 174 of the March/April issue.

Future Articles continued from p. 303

A Combination Flame Atomic Fluorescence–Atomic Emission dc Spectrometer for Analysis of Trace Wear Metals in Jet Engine Oils—R. L. Miller, L. M. Fraser, and J. D. Winefordner.

The Spectrographic Determination of Traces of Tellurium—R. Cone, E. Leao, and J. Marks.

Compositional Determination of Sputtered Tantalum–Aluminum Thin Films—J. A. Nohe and D. A. Green.

Machine Intelligence Applied to Chemical Systems. A Graph Theoretical and Learning Machine Study of Second Order Effects in Low Resolution Mass Spectra—P. Jurs.

Notes

Monomeric OH Stretching Frequencies in Monohalogenated Monocarboxylic Acids—J. E. Katon and D. Sinha.

International Standardization in Mössbauer Spectrometry—P. A. Pella and J. R. DeVoe.

Spectroscopic Techniques

A Cell for Resonance Raman Excitation with Lasers in Liquids—W. Kiefer and H. J. Bernstein.

Microsampling for Infrared and Emission Analyses—P. wh. Schuessler.

A Cylindrical Sector Driven by Either Water or Air—J. W. Mellichamp and L. L. Wilcox.

Cold Pressing Solid Samples in a Wax Disk for Far Infrared Analysis—M. E. Peterkin.

Microspectrophotometer Cells of Fused Construction—W. T. Carnall and P. R. Fields.